applied sciences

MDPI

Article

Parametric Investigation of Corner Effect on Soil Nailed Walls and Prediction Using Machine Learning Methods

Semiha Poyraz [1,2,*] and İsa Vural [3]

[1] Graduate Education Institute, Sakarya University of Applied Science, 54100 Sakarya, Turkey
[2] Vocational School, Bilecik Seyh Edebali University, 11100 Bilecik, Turkey
[3] Faculty of Technology Civil Engineering, Sakarya University of Applied Science, 54100 Sakarya, Turkey; ivural@subu.edu.tr
* Correspondence: semiha.poyraz@bilecik.edu.tr; Tel.: +90-228-214-1336

Abstract: The performance of soil nailed walls is evaluated based on lateral displacements, especially in high walls. In this study, the displacement behavior of nailed walls, which are frequently preferred in retaining wall systems in hard clayey soils, was examined by taking into account the corner effect. The nailed wall model was created using Plaxis 2D v.23, and the performance of the model was verified with the results of inclinometer measurements taken on-site. To assess the influence of excavation pit dimensions on the corner effect, 25 three-dimensional and 25 plane–strain slice models were created using Plaxis 3D v.23, and the effect of excavation pit dimensions on the plane–strain ratio (PSR) was determined. Then, analysis studies were carried out by creating 336 3D and 336 plane–strain slice models with variable parameters, such as slope angle (β), wall angle (α), nail length (L/H), excavation depth (H), and distance from the corner (xH). Its effects on PSR were determined. The interactions of the parameters with each other and PSR estimation were evaluated using machine learning (ML) methods: artificial neural networks (ANN), classifical and regression tree (CART), support vector regression (SVR), extreme gradient boosting (XGBoost). The proposed ML prediction methods and PSR results were compared with performance metrics and reliable results were obtained.

Keywords: corner effect; finite element analysis; lateral displacement; machine learning; PSR; soil nailed wall

Citation: Poyraz, S.; Vural, İ. Parametric Investigation of Corner Effect on Soil Nailed Walls and Prediction Using Machine Learning Methods. *Appl. Sci.* **2024**, *14*, 7331. https://doi.org/10.3390/app14167331

Academic Editor: Wei Gao

Received: 21 July 2024
Revised: 11 August 2024
Accepted: 12 August 2024
Published: 20 August 2024

1. Introduction

The strain that occurs during deep excavations causes lateral displacements [1–4]. The soil nail technique in deep excavation works has gained popularity in recent years due to its effectiveness and cost-efficiency in providing support across various ground conditions. In the design of soil nailed walls, it is crucial to estimate the maximum lateral displacements during the design phase, particularly under conditions where this issue is significant. Recommended models for estimating lateral displacements are available and have been incorporated into soil nailed wall design guides [5–9].

Researchers have extensively investigated the displacement behavior of soil nailed walls, employing both numerical and experimental methods [10–13]. Yuan et al. conducted a statistical analysis by creating a lateral and vertical displacement database from measurements obtained from different soil nailed wall projects. They concluded that the displacements used in the design guides were higher than field measurements [14]. Moreover, Esmaeili et al. utilized close-range photogrammetry with the combined photogrammetry displacement adjustment (CPDA) method for the first time in a building project excavation to determine displacements in soil nailed walls [15]. The geometric features of soil nailed walls also have an effect on displacements [16,17]. Case-based probabilistic studies have also been conducted on the studied wall system. Additionally, case-based, probabilistic studies, such as Monte Carlo simulation, have been conducted on the nailed wall system [18].

Numerical-based models have been widely used in research on soil nailed walls, particularly over the last three decades. Finite element (FE) software stands out as one of the widely used and reliable tools in this domain [19]. It provides results that are consistent with those of field measurements, laboratory experiments, limit equilibrium methods, and various numerical techniques [20–23]. For example, in one of these studies, the construction stages and soil pressure during the application process of soil nails were comparatively examined under laboratory conditions and using Plaxis v.23 software, and compatible results were obtained. [24]. Similarly, in another study focusing on the mechanical behavior of soil nailed walls, consistent results were achieved through both experimental and numerical investigations [25]. In the research conducted on soil nailed walls, the strength reduction method (SRM), which is a deterministic approach, was examined comparatively with the finite element method (FEM), and compatible results were obtained [26].

The excavation environment is a three-dimensional environment by nature. Excavation corners have effects on displacements and stresses. Researchers have conducted studies on different shoring systems to investigate these effects. The expression plane–strain ratio (PSR) is used in excavation pits to describe the change in displacements according to the distance from the corner (corner effect). It is defined as the ratio between the maximum displacements obtained from the three-dimensional analysis and two-dimensional analysis of a section at a certain distance of from the corner [27]. There have been corner effect studies on different retaining wall systems. The PSR value was estimated by comparing the three-dimensional effect with 3D finite element analysis in a deep excavation supported by a diaphragm wall [28]. Another study investigated the corner effect in deep excavation work using soil nails, depending on whether the excavation pit is square, concave, or convex [29]. In a different study, an optimum design was made for a soil nailed wall–pile–anchor cable support system in deep excavation, taking into account the corner effect [30].

Empirical and theoretical models remain inadequate for accurately predicting displacements in soil nailed walls. While database performance is strong, the ability to generalize to unseen data still needs further improvement. This deficiency confirms that various properties of soils can differ greatly, even for those taken from the same place. Therefore, geotechnical problems require learning strategies such as machine learning, which can take advantage of multiple predictors and their fundamental properties [31]. These complex situations can be handled with machine learning (ML). Machine learning has established an excellent field for itself in the geotechnical field, as it copes even with distorted, fuzzy, and incorrect data [32].

Various ML-based models are used for geotechnical problems, including machine learning methods for displacement estimation and prediction, as well as optimization studies in soil nailed walls. In a study, the structural risk minimization-multi-gene genetic programming (SRM-MGGP) method was proposed using support vector regression (SVR), artificial neural networks (ANNs), and multi-gene genetic programming (MGGP) methods to formulate the mathematical relationship between cohesion, friction angle, nail slope, nail length, and slope height, and to estimate the safety factor (Garg et al., 2014). In another study, the optimum slope, spacing, and nail length/wall height of single-row vertical nails in soil nailed walls were analyzed using Plaxis 2D v.23. Then, a comparative optimization study was conducted with Taguchi's design of experiment (DOE), genetic algorithm (GA), and particle swarm optimization (PSO) [33].

To summarize, in the first stage of this study, the factors that may have an impact on the corner effect in soil nailed walls were investigated in many aspects. For this purpose, three-dimensional and two-dimensional models were created using Plaxis v.23 software, a finite element software program, and the performance of the model was compared with inclinometer measurements. Then, the effect of excavation pit dimensions on the corner effect was investigated. After the excavation pit dimensions were determined, the parametric research phase began. Analysis studies were carried out by creating 336 3D models and 336 plane–strain slice models with variables including slope angle (β), soil nailed wall angle (α), nail length (L/H), and excavation depth (H), to determine the plane–

strain ratio (PSR). In the second stage of this study, PSR prediction was performed using machine learning methods. It is very difficult to make predictions with simple statistical methods, especially in studies with crowded data sets. Predictions made with machine learning methods can produce reliable results, especially in complex and large-volume data. As a result of this study, analysis studies were carried out with machine learning methods due to the large number of PSR data obtained and the non-linearity of the obtained results. There are many methods for machine learning. This is necessary because there is no method that works perfectly on every data set. For this reason, prediction studies have been carried out using more than one method. The methods that are most preferred in the literature provide reliable results. This study aims to reveal the most reliable results obtained from the predictions made by the methods. Artificial neural networks (ANNs), support vector regression (SVR), extreme gradient boosting (XGBoost), and classifical and regression tree (CART) prediction models were used for PSR prediction, and their performances were compared using various metrics.

2. Machine Learning Methods

2.1. Artificial Neural Networks (ANNs)

Artificial neural networks (ANNs), developed by researchers including Hopfield, Rumelhart, and Grossberg, are computational models designed to emulate the functioning of biological neural networks [34–37]. ANNs are now also used in other engineering fields [38]. The method consists of a series of interconnected nodes or "neurons" (input variables) that process information in parallel. Neurons consider a linear combination of inputs, apply an activation function, and pass the output layers (responses) to the neurons below (Figure 1).

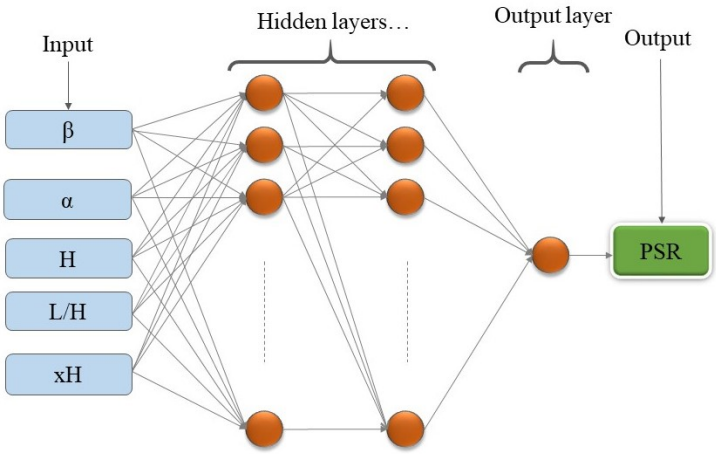

Figure 1. ANN configurations selected as the prediction model for the PSR response.

2.2. Classifical and Regression Tree (CART)

Classifical and regression tree (CART), a random forest (RF) method, has been frequently used in prediction studies in recent years due to its superior data classification ability [39,40]. For regression problems, the output variables are fitted using samples of input variables. For each of the input variables, the data are divided into several points. For predicted and actual values, the sum of square error (SSE) is calculated at each split point, selecting the minimum SSE at the node [41]. In Equation (1), the expression $\hat{h}_{RF}(x)$ in the prediction function $\hat{h}(x, \theta_i)$ indicates the model's prediction of the target. A typical CART pattern estimation scheme is shown in Figure 2.

$$\hat{h}_{RF}(x) = \frac{1}{q}\sum_{i=1}^{q} \hat{h}\,(x, \theta_i) \tag{1}$$

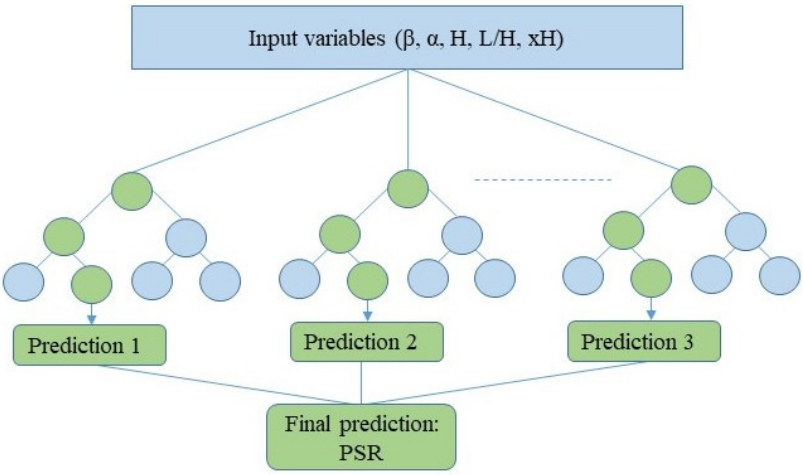

Figure 2. Schematic diagram of the CART.

2.3. XGBoost

Extreme gradient boosting (XGBoost) is an improvement to gradient boosting [42]. The XGBoost algorithm uses the classifical and regression tree (CART) algorithm to create trees. Notably, XGBoost base predictors can encompass not only decision trees, but also other machine learning (ML) models. In this study, regression trees were used as basic predictors. As outlined in Equations (2) and (3), the aim is to reduce the loss function by iteratively adding weak models to the ensemble to generally correct the errors made by previous models [43–46].

$$L_{xgb} = \sum_{i=1}^{N} L(y_i, F(x_i)) + \sum_{m=1}^{M} \Omega(h_m) \quad (2)$$

$$\Omega(h) = \gamma T + \frac{1}{2}\lambda \|w\|^2 \quad (3)$$

2.4. SVR

Support vector regression (SVR) originates from the support vector machines (SVM) method used in data research [44,47,48]. Unlike traditional statistical regression methods, SVR disregards statistical assumptions and manipulates data to create nonlinear models (Figure 3). Another distinction lies in its ability to bypass statistical assumptions and manipulate data to form nonlinear models [49].

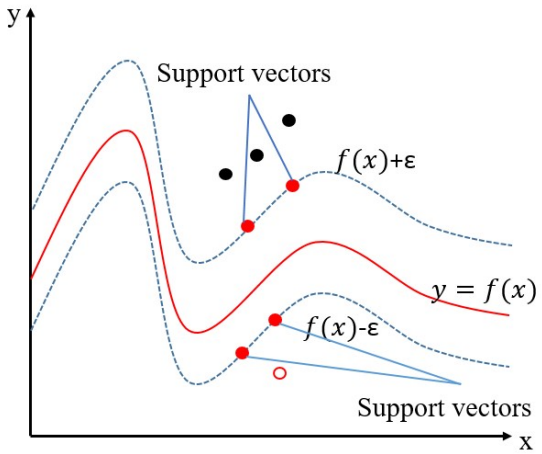

Figure 3. Typical kernel radial basis functions of SVR.

3. Materials and Methods

3.1. Database of Soil Nailed Wall

Soil nailed walls are generally applied to hard clay, medium hard clay, dense sand, and medium-dense sand soils. As part of the excavation work for the Tepe Shopping Mall project in Istanbul, Türkiye, soil nailed walls were implemented (Figure 4a,b). The displacement measurements used in this study were obtained from Inclinometer-4 (Figure 4c). General information regarding the soil nailed wall, specifically applied to hard clay soil by Zetaş A.Ş., along with its geometric properties, is presented in Figure 5 and Table 1 [50]. The nail lengths did not change with depth and were kept constant.

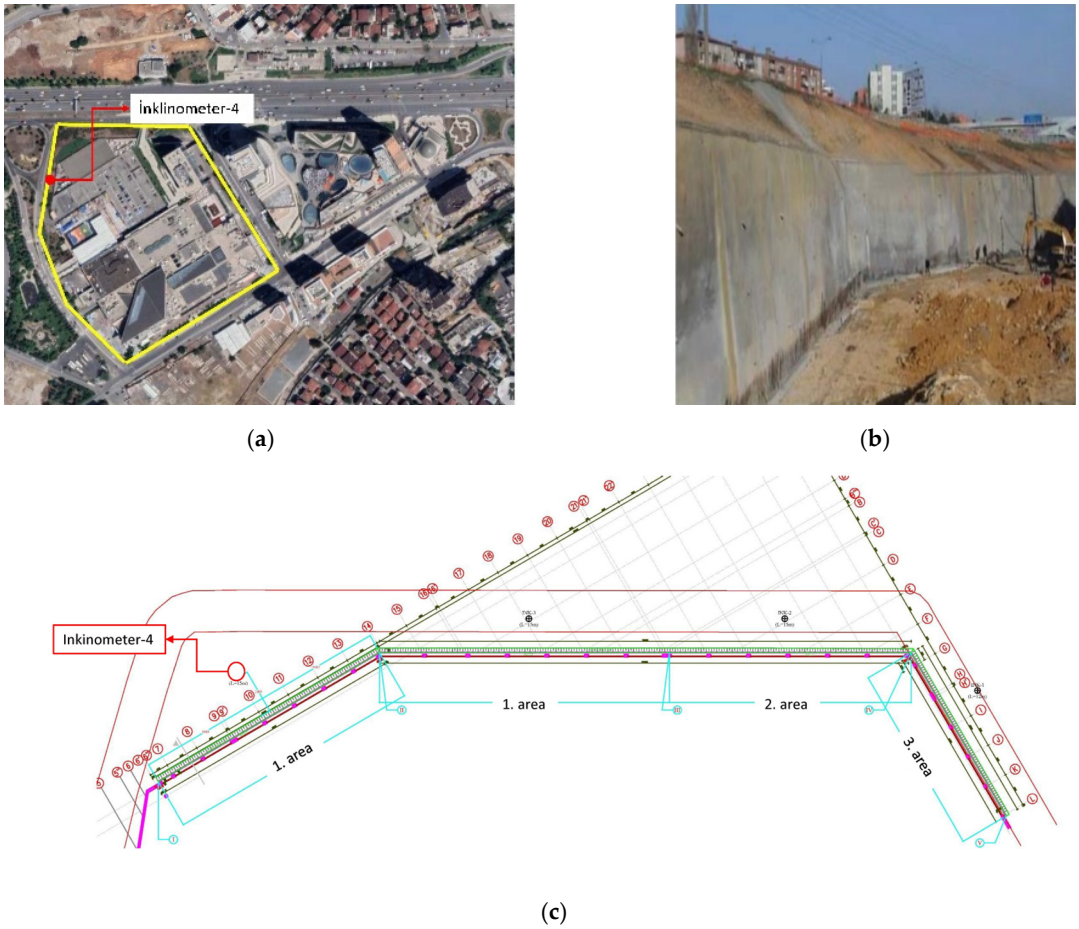

Figure 4. Tepe Shopping Mall project and soil nailed wall application: (**a**) general view; (**b**) first row nail application; (**c**) soil nail application plan.

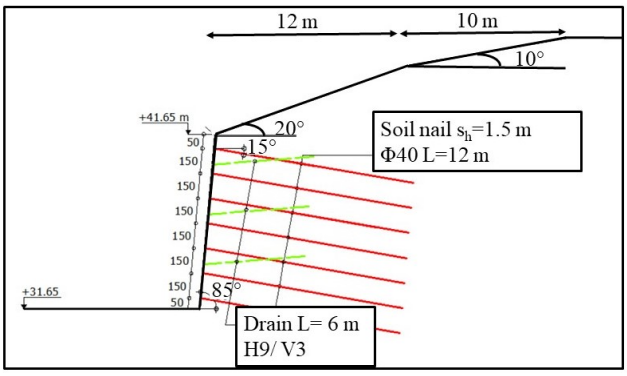

Figure 5. Tepe Shopping Mall project soil nailed wall section.

Table 1. Geometric information of Tepe Shopping Mall project.

Soil Nailed Wall H (m)	Soil Nail Impact Area $S_h \times S_v$ (m^2)	Soil Nailed Wall Angle α (°)	Soil Nail Angle ω (°)	Soil Nail Length L (m)	Nail Diameter D (mm)
10.0	1.5 × 1.5	85	15	12	105

3.2. Finite Element Model Presentation and Verification of the Model with Field Measurement Results

The soil parameters applied based on the Plaxis 2D v.2023 and Plaxis 3D v.2023 finite element models in the soil nailed walls in the Tepe Shopping Mall project are given in Table 2 [51,52].

Table 2. Plaxis 2D and Plaxis 3D Tepe Shopping Mall project soil properties.

Soil	Soil Model	Unit Volume Weight (kN/m^3)	Friction Angle φ' °	Cohesion c (kPa)	E_{50}^{ref} kN/m^2	E_{oed}^{ref} kN/m^2	E_{ur}^{ref} kN/m^2	ν_{ur}	R_{inter}
Soil 1	Hardening soil	19	25	15	53,000	53,000	159,000	0.25	0.67

A soil nail is a composite element composed of nails and cement grout. In finite element models, the soil nail is defined as an embedded beam object. The embedded beam represents the soil nail in the best way since it is an object consisting of beam elements that interact with the soil and body friction through special interface elements. In addition, in soil nail applications, the application surface is often covered with sprayed concrete and this representative element is designated as plate. The properties of embedded beam and plate elements for Plaxis 2D and Plaxis 3D models are given in Table 3.

Table 3. Plaxis 2D and Plaxis 3D Tepe Shopping Mall project soil nail and shotcrete parameters.

FE	Soil Nail	E (kN/m^2)	γ (kN/m^3)	D (m)	Bond Strength (kPa)	Axial Skin Resistance	T_{skin}, Start, Max	T_{skin}, End, Max	Material
Plaxis 2D	Embedded Beam	93.00×10^6	1	0.105	300	Linear	98.96	98.96	Rock bolt, Rigid
Plaxis 3D	Embedded Beam	93.00×10^6	1	0.105	300	Linear	98.96	98.96	Rock bolt, Rigid
FE	**Shotcrete**	**Material Type**	**γ (kN/m^3)**	**d (m)**	**EA_1 (kN/m)**	**E_1 (kN/m^2)**	**EI (kNm^2/m)**	**V_{12}**	**Interface**
Plaxis 2D	Plate	Elastic	1.2	0.200	4.200×10^6	21.00×10^6	14.00×10^3	0.2	Defined
Plaxis 3D	Plate	Elastic	1.2	0.200	-	21.00×10^6	-	0.2	Defined

In order to investigate lateral displacements, 2D analysis was first performed using Plaxis 2D finite element software, and performance reliability was confirmed with field inclinometer-4 measurement results (Figure 6). Then, a plane–strain slice model was created using Plaxis 3D finite element software. Plaxis 2D analyses give larger displacements than Plaxis 3D analyses, with slight differences. In creating 3D models, Plaxis 3D plane–strain slice model parameters with proven model accuracy were used.

3.3. Method

Within the scope of the study method, the accuracy of the Plaxis finite element model was ensured in the first stage. Then, the corner effect of the excavation pit dimensions was investigated using Plaxis 3D. Excavation pit dimensions were preferred to be rectangular in parametric studies. Conditions in which the walls of the entire excavation pit perimeter were also soil nailed walls were evaluated. The second phase of the parametric research on fixed excavation pit dimensions was initiated. At this stage, the effects of slope angle,

wall angle, excavation depth, nail length, and distance from the corner variables on plane–strain ratio (PSR) were determined using Plaxis 3D. The PSR prediction study was carried out using machine learning models: extreme gradient boosting (XGBoost), classifical and regression tree (CART), support vector regression (SVR), and artificial neural networks (ANNs), and the reliability of the models was checked (Figure 7).

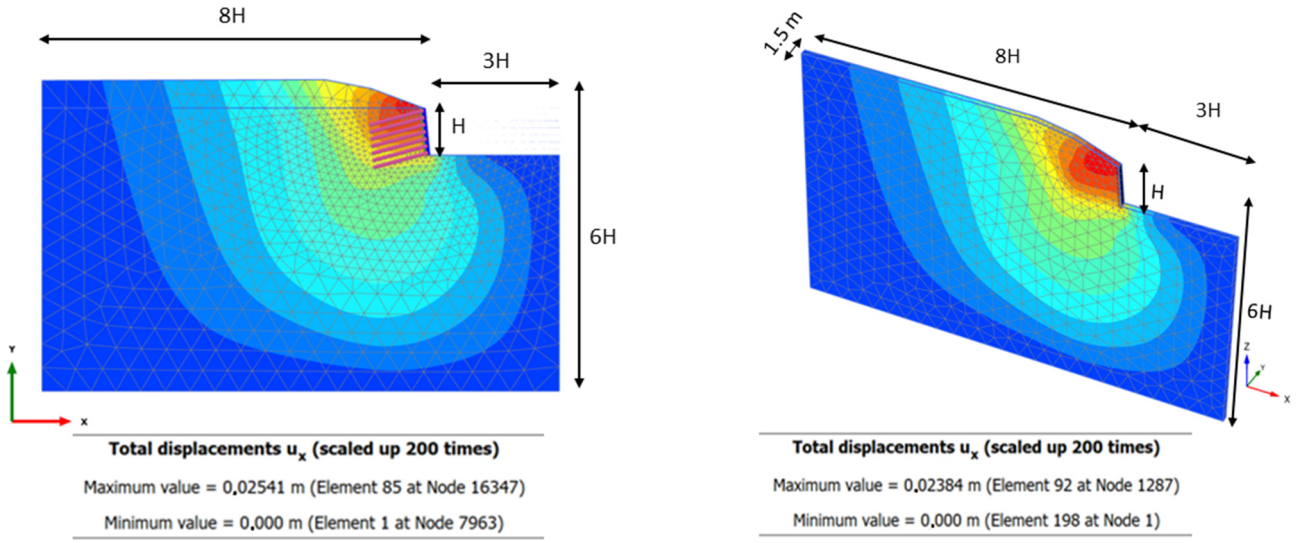

(**a**) (**b**)

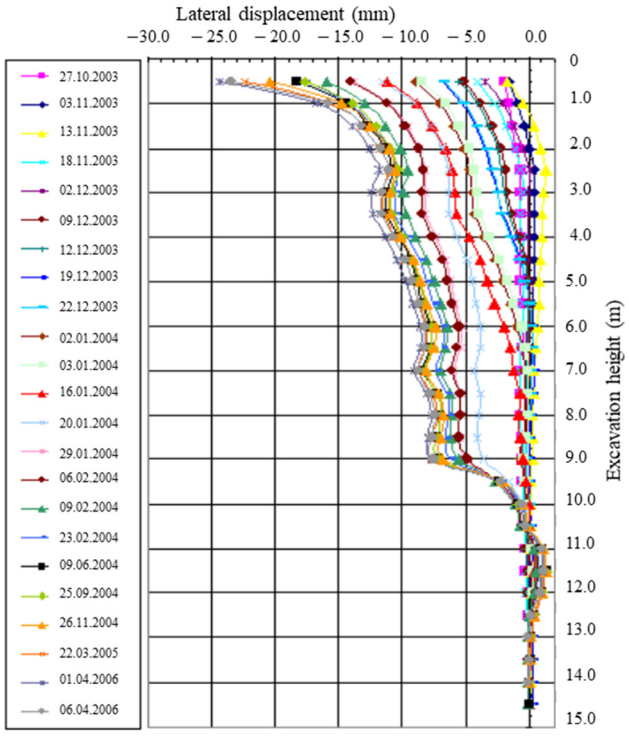

(**c**)

Figure 6. Comparison of lateral displacements using Plaxis 2D, Plaxis 3D plane–strain model, and field measurement: (**a**) Plaxis 2D analysis; (**b**) Plaxis 3D plane–strain slice model analysis; (**c**) Inklinometer-4 measurement.

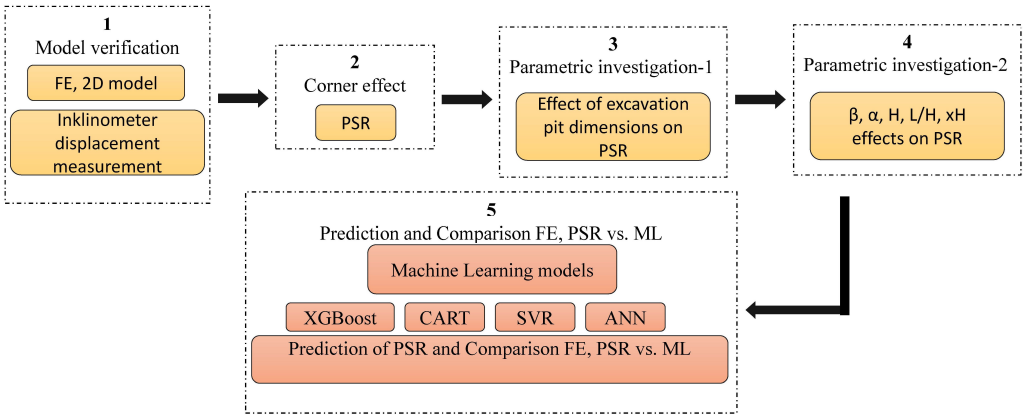

Figure 7. General flowchart of research on the relationship between PSR and parametric factors.

3.4. Corner Effect (PSR)

A new parameter called the plane–strain ratio (PSR) was introduced by Ou et al. in 1996 to describe lateral displacement behavior. The PSR value is expressed as the ratio of the maximum lateral displacements in three-dimensional analyzes $(3D\ \lambda_{hmax})$ to the maximum lateral displacements in two-dimensional analyses $(2D\ \lambda_{hmax})$ (Equation (4)). As the PSR value increases, sections less affected by corners emerge. Based on the aspect ratio for the excavation geometry and the distance from the corner, if the PSR value is close to 1, it means that the corner effect is negligible [27,53,54].

$$PSR = 3D\ \lambda_{hmax} / \ 2D\ \lambda_{hmax} \quad (4)$$

4. Results and Discussion

4.1. Parametric Investigation

Within the scope of the parametric research, factors that may affect the lateral displacements of the soil nailed wall were discussed. In this context, the research is discussed in two parts. In the first part, the effects of the excavation pit dimensions on the plane–strain ratio (PSR) were investigated. In the second part, the effects of slope angle (β), wall angle (α), excavation depth (H), and nail length (L/H) conditions on PSR were examined via Plaxis 3D software analysis studies. The excavation area geometry was determined as rectangular in parametric studies. Although the average time in parametric studies varies depending on the model size and the number of nails, a single three-dimensional analysis took an average of 15 h. The analysis time of all three-dimensional models was approximately 300 days.

4.2. Effect of Excavation Pit Dimensions on PSR

Excavation geometry and soil parameters were taken from the Tepe Shopping Mall case. In the investigation of the excavation pit dimensions, the slope angle (β) was accepted as zero, the nail length was taken as half of the excavation depth, and the effect of the change in the excavation dimensions (B and L) on the plane–strain ratio (PSR) behavior was examined. The excavation pit dimensions consisted of the primary wall length (L) and secondary wall length (B). The model boundary conditions were taken as three times the excavation widths, and attention was paid to the boundary conditions. The model depth was taken as six times the excavation depth (Figure 8).

Excavation pit parametric dimensions were determined as multiples of the excavation depth (H). To investigate the dimensions of the excavation pit, 25 Plaxis 3D models and 25 Plaxis 3D plane–strain models were created and analyzed (Table 4).

In the analysis studies, it was seen that different B conditions had no effect on plane-strain ratio (PSR) changes under the same primary wall length (L) length conditions. Under the same secondary wall length (B) conditions, the PSR value remained at low values, at most approximately 0.65, in the L length 2H condition. Under the same B conditions,

similar behavior was observed as the L length 4H, 6H, 8H, and 10H PSR graphs moved away from the corner, and the PSR value reached 0.90 after approximately 3H (Figure 9). In research on the corner effect of excavation pit dimensions, the presence of the corner effect becomes more evident, especially in short-sized retaining walls [27,53].

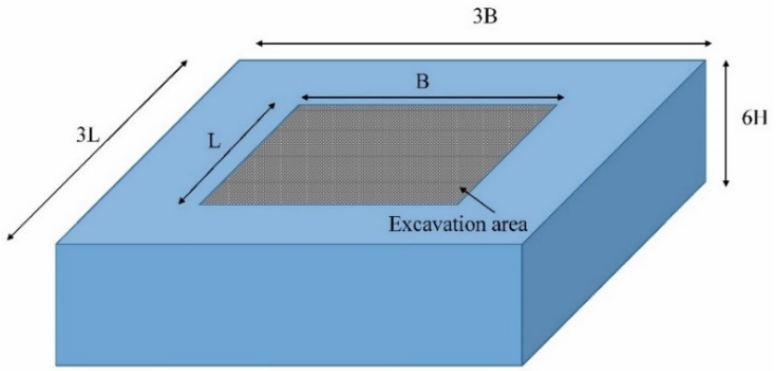

Figure 8. Plaxis 3D excavation pit and model dimensions.

Table 4. Excavation pit dimensions.

	Group 1	Group 2	Group 3	Group 4	Group 5
	B1 = 2H	**B2 = 4H**	**B3 = 6H**	**B4 = 8H**	**B5 = 10H**
L-1	2H	2H	2H	2H	2H
L-2	4H	4H	4H	4H	4H
L-3	6H	6H	6H	6H	6H
L-4	8H	8H	8H	8H	8H
L-5	10H	10H	10H	10H	10H

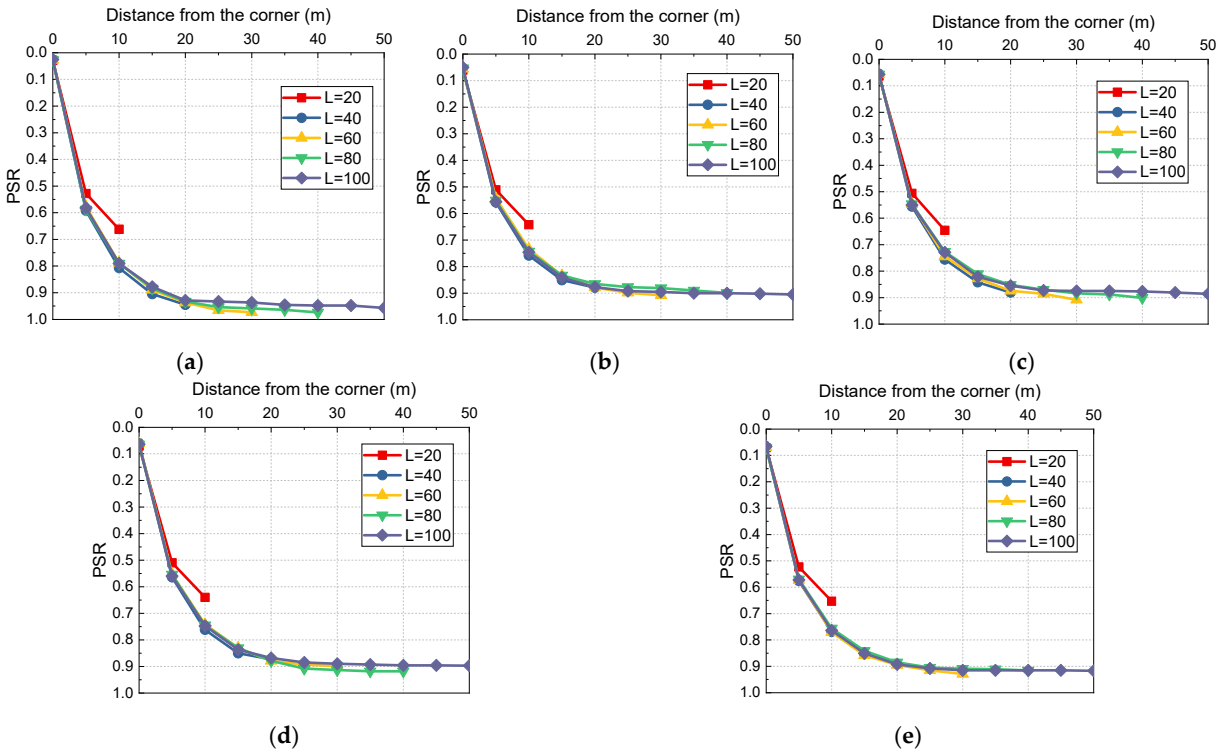

Figure 9. PSR changes depending on primary and secondary wall lengths: (**a**) B = 20 m; (**b**) B = 40 m; (**c**) B = 60 m; (**d**) B = 80 m; (**e**) B = 100 m.

4.3. Effects of Slope Angle (β), Wall Angle (α), Excavation Depth (H), Nail Length (L/H), and Distance from Corner (xH) on PSR

There are many controversial studies on the corner effect of shoring structure type, soil type, and excavation pit dimensions [3,27,53,55]. There are limited studies on how variables such as the back slope angle (β), nailed wall angle (α), nail length (L/H), and excavation depth (H) affect the corner effect in nailed walls. At this stage of the study, the effects of the specified factors on the plane–strain ratio (PSR) were investigated. The nail length was kept constant throughout the depth. The width of the slope angle was determined as two times the width of the excavation depth (2H), since the displacement increase rate did not change significantly after 2H distance. A total of 336 3D models and 336 plane–strain slice models were created using the parametric variables shown in Figure 10, and displacement analysis studies were carried out.

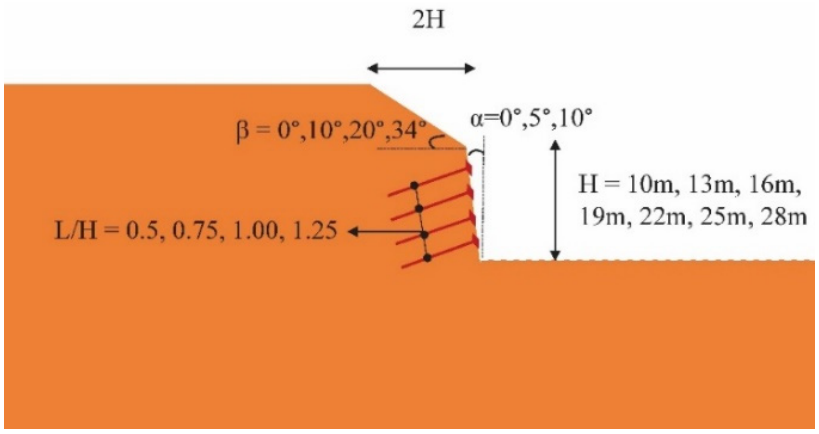

Figure 10. Parametric variables and properties based on Plaxis 2D and Plaxis 3D models.

In Plaxis 3D models, the primary wall (L) and secondary wall (B) distances of the excavation pit are kept equal (B = L). This is because the length of the secondary wall (B) has no effect on the primary wall (L) displacements (Figure 9). Additionally, no significant change in the plane–strain ratio (PSR) was observed after 3H distance. Therefore, B = L = 6H excavation dimensions were chosen in all Plaxis 3D models (Figure 11a). Since the lateral distance between the nails was 1.5 m in this case, the width was kept constant at 1.5 m in all 3D and plane–strain slice models (Figure 11b). While creating models in analysis studies, dimensions were determined by taking boundary conditions into account (Figure 11).

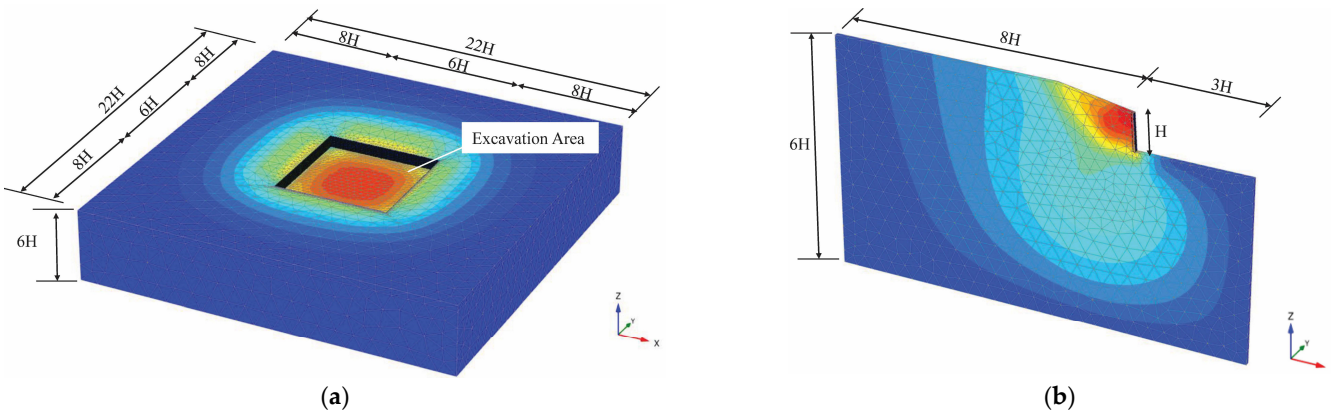

(**a**) (**b**)

Figure 11. Finite element model for the reference for the calculation of the PSR: (**a**) 3D model; (**b**) 3D plane–strain slice model.

A total of 336 3D models and 336 plane–strain slice models were analyzed for corner effect research based on five variable conditions on nailed walls. The change in plane–strain ratio (PSR) values was calculated for each excavation depth at distances from the corner of 0, 0.5, 1.0, 1.5, 2.0, 2.5, and 3.0 times the excavation depth, and graphs were created. During the plane–strain slice model analyses, 106 models collapsed, and during the 3D model displacement analyses, 89 models collapsed. The PSR values based on the non-collapse lateral displacement analysis results are presented in Figure 12, with a total number of 1610 data points.

As seen in Figure 12, depending on the distance from the corner, the plane–strain ratio (PSR) value was approximately 0.1 at the corner under back slope angle $\beta = 0^{\circ}$ conditions. However, this value increased to 0.50 at a distance of 0.5H from the corner and even reached values as high as 0.80 with increasing nail length. At 1H and beyond, the rate of increase in PSR decreased, and the values approached maximum levels earlier with the increases in nail length and wall angle. With the increase in β, the PSR value at the corner also increased, and depending on the increase in nail length (L/H) and wall angle (α), the PSR value in the corner increased up to 0.50.

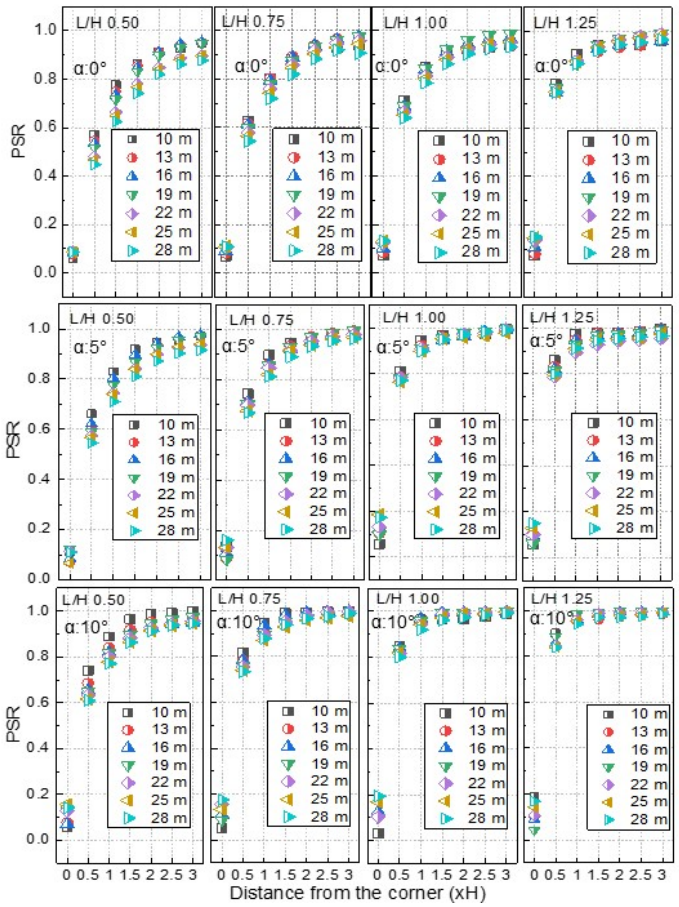

(**a**)

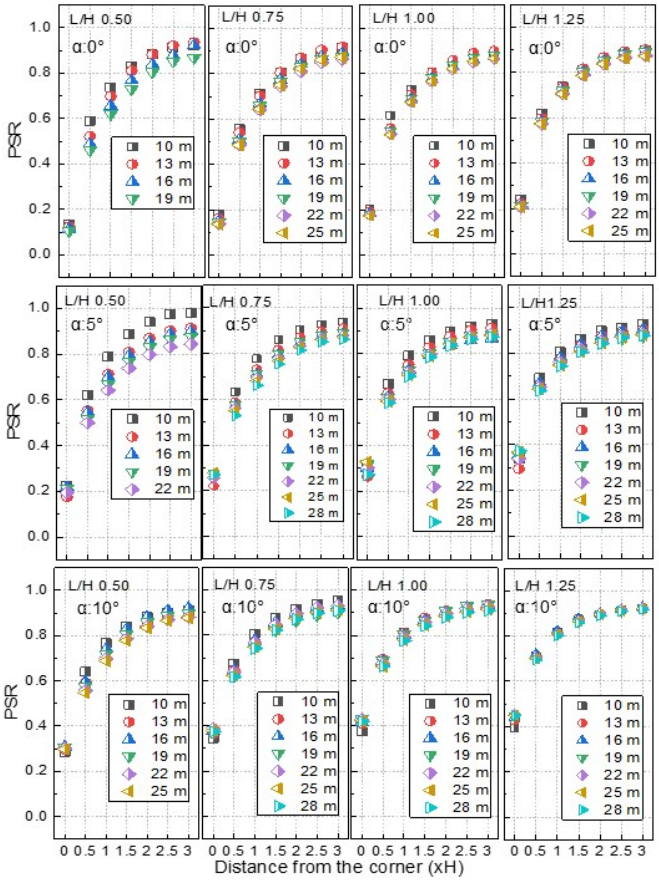

(**b**)

Figure 12. *Cont.*

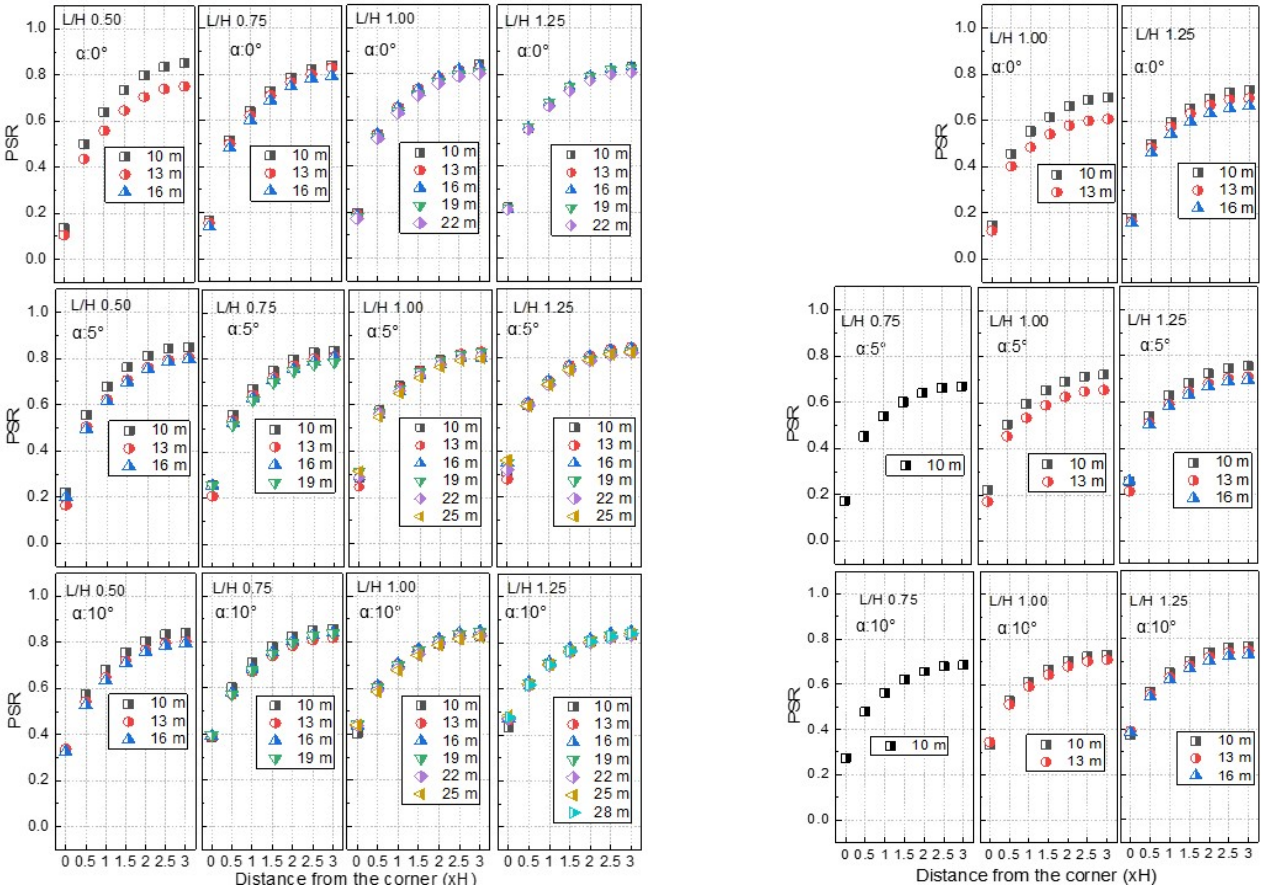

Figure 12. PSR changes in nailed walls under different slope angle (β), wall angle (α), excavation depth (H), and nail length (L/H) conditions; (**a**) β = 0° (**b**) β = 10° (**c**) β = 20° (**d**) β = 34°.

At distances from the same corner, the plane–strain slice (PSR) value decreased as the back slope angle (β) increased, and reached maximum values again at farther distances as β increased. While the PSR value was approximately 0.1 at the corner under β = 0° conditions, it approached 1 as it moved away from the corner. It can be observed that the PSR value reached 0.90 at most when the β value was 10°, 0.80 at 20°, and 0.70 at 34°. Increasing β led to a decrease in the PSR value, thereby increasing the corner effect. As the wall angle (α) increased, the PSR value approached the maximum value at shorter distances from the corner under β = 0° conditions [56]. This situation becomes more evident as the nail length increases (Figure 12a). In the case of β = 10°, increasing the α angle brought the PSR curves, which changed with depth, closer to each other (Figure 12b). The fact that the PSR curves approached each other with depth was also observed under other β (20°, 34°) conditions (Figure 12c,d). The effect of increasing the α angle on PSR gradually decreased with the increase of the β angle. Under β = 0° conditions, as the excavation depth increased, the PSR value decreased, thus increasing the corner effect. While increasing the excavation depth clearly showed the decrease in PSR in the case of β = 0°, increasing the β angle caused this effect to decrease and the PSR curves became closer to one another. In a study conducted by Tabur in 2014, it was observed that the corner effect continued to affect areas farther away as the excavation depth increased in hard clay soils [57]. While the effect of nail length on PSR remained at lower values in the case of β = 0° and nail length L/H = 0.50, as the nail length increased, PSR progressed to higher values and approached 1. Additionally, with increasing nail length, higher PSR results were obtained at the same distance from the corner under the same β conditions, indicating a reduction in the corner effect. An increase in the β angle decreased the effect of nail length on PSR. As the stiffness increases

in nailed walls, the corner effect decreases. Increasing the slope angle (β) and excavation depth (H) increases the corner effect because it causes a decrease in the stiffness of nailed walls. Increasing the nail length (L/H) and wall angle (α) will increase the stiffness, thus increasing the PSR value and decreasing the corner effect [29,58].

4.4. Correlation Analysis

Based on the distribution of the variables, the coefficients between the Pearson correlation and direction and strength of the monotonic relationship between the two parameters were calculated pairwise and shown as a heat map (Figure 13). All data (1610) regarding distance from the corner (xH), nail length (L/H), excavation depth (H), wall angle (α), slope angle (β), and plane–strain ratio (PSR) data were evaluated together.

Figure 13. Pearson correlation with heat map.

The correlation effect rates and their meanings are provided in Table 5. There is a very strong positive relationship between PSR and xH. There is a negative relationship between PSR and β, a negative relationship between β and H, and a weak, positive relationship between β and L/H.

Table 5. Correlation effect rates and their meanings.

Correlation Coefficient	Description	Parameters
0.80–1.00	Very strong	PSR vs. xH
0.60–0.79	Strong	-
0.40–0.59	Moderate	-
0.20–0.39	Weak	PSR vs. β, β vs. H, β vs. L/H, L/H vs. xH, H vs. xH, α vs. L/H, α vs.
0.00–0.19	Very weak	H, β vs. α, PSR vs. α, H vs. L/H, PSR vs. H, PSR vs. L/H, β vs. xH, α vs. xH

5. Machine Learning Models

5.1. Hyperparameters Configuration

Hyperparameters play a crucial role in determining the prediction performance of machine learning algorithms. Therefore, it is critical to tune the hyperparameters correctly. One of the traditional approaches commonly used today is grid search. First, a Cartesian product of all hyperparameter combinations of plausible values is generated. Afterward, the machine learning (ML) algorithm performs data training for all hyperparameter combinations. Training performance is measured by the cross-validation technique [59,60]. In this study, the grid search method was employed to adjust the hyperparameters. To train the ML model, the training and test datasets must be represented correctly. Determining the appropriate ratio between the test dataset and the training dataset is a critical aspect, with ongoing discussions in the field. In practice, ratios such as 70:30 and 60:40 are used [61]. A

training–test split ratio of 70:30 was adopted, along with the layered learning technique. Then, cross-validation was performed. The optimized hyperparameters used to estimate the machine learning models used in this study are provided in Table 6.

Table 6. Optimized hyperparameters used to predict ML models.

ML	Parameters	Value
XGBoost	Number of estimator	200
	Maximum depth	5
	Minimum child weight	1
	Learning rate	0.1
SVR	Support vectors	117
	Cost	100
	Epsilon	0.1
	Gamma	0.01
	Kernel	Radial basis functions
CART	Max. depth	None
	Min. samples leaf	2
	Min. samples split	5
ANN	Hidden layer size	2
	Neurons	20 + 20

5.2. Performance Metrics

The ideal prediction parameters and value ranges are provided in Table 7. The specified performance metrics were used to evaluate the performance of the models used in plane–strain ratio (PSR) prediction.

Table 7. Performance metrics [62].

No	Parameter	Equation
1	Coefficient of determination (R^2)	$R^2 = \frac{\sum_{i=1}^{n}(y_i - y_{mean})^2 - \sum_{i=1}^{n}(y_i - \hat{y}_i)^2}{\sum_{i=1}^{n}(y_i - y_{mean})^2}$
2	Mean absolute error (MAE)	$MAE = \frac{1}{n}\sum_{i=1}^{m}\lvert(\hat{y}_i - y_i)\rvert$
3	Root-mean-square error (RMSE)	$RMSE = \sqrt{\frac{1}{N}\sum_{i=1}^{n}(y_i - \hat{y}_i)^2}$

5.3. Evaluation of Machine Learning Model Prediction Performances

This section discusses models created to predict an output using five input variables, along with their corresponding results. Models created to predict an output using five input variables are discussed with their results in this section. The relevant prediction results are shown in detail in Table 8. The performance of the models in predicting training and testing outcomes was evaluated. The analysis results showed that the classifical and regression tree (CART) and extreme gradient boosting (XGBoost) models exhibited the highest R^2 (0.99) and lowest RMSE (0.00) values for plane–strain ratio (PSR) prediction during training. The test results regarding prediction ability were R^2 0.99 with XGBoost and R^2 0.98 with CART. RMSE of 0.01 was obtained for XGBoost and 0.02 for CART. However, artificial neural networks (ANNs) and support vector regression (SVR) models demonstrated comparatively lower performance compared with other prediction models.

The plane–strain ratio (PSR) prediction and finite element (FE) PSR relationships of the prediction models are illustrated in Figure 14. While the ideal fit is given as a dark blue line, the ±20% error rate range is also indicated on the graphics. Among the prediction models, artificial neural networks (ANNs) and support vector regression (SVR) tend to make errors. Therefore, extreme gradient boosting (XGBoost) and classifical and regression tree (CART)

can be recommended as the prediction models. The superiority of the proposed prediction models (XGBoost and CART) compared with other traditional models (ANN and SVR) is clearly evident.

Table 8. Comparison of model performance.

Indicator Models Used	R^2		MAE		RMSE	
	Training	Test	Training	Test	Training	Test
ANN	0.95	0.91	0.05	0.05	0.06	0.07
SVR	0.92	0.91	0.05	0.06	0.06	0.07
CART	0.99	0.98	0.00	0.01	0.01	0.02
XGBoost	0.99	0.99	0.00	0.01	0.00	0.01

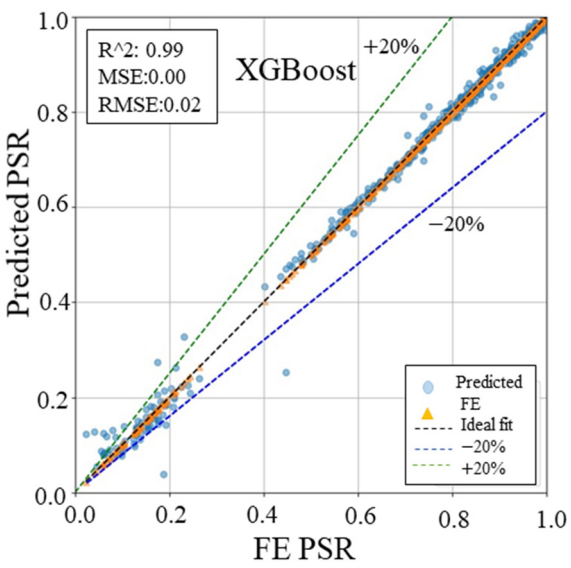

(**a**)

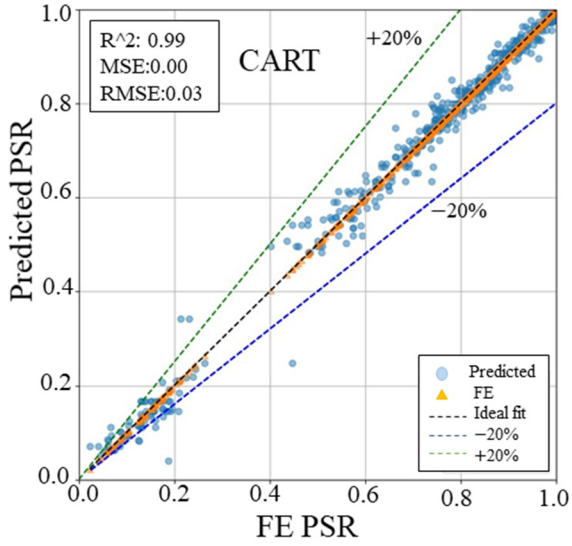

(**b**)

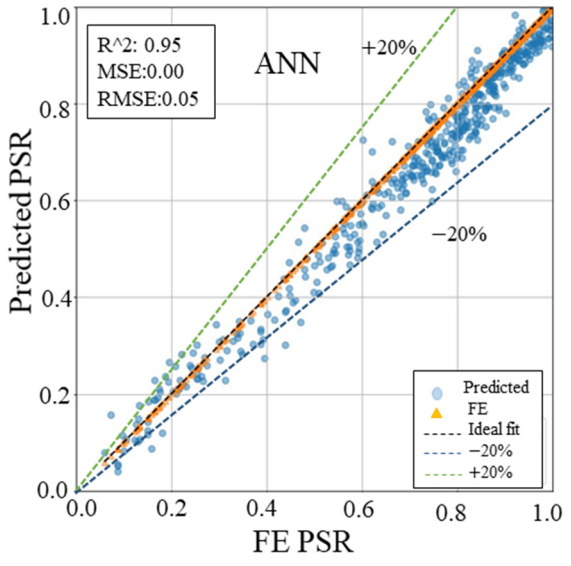

(**c**)

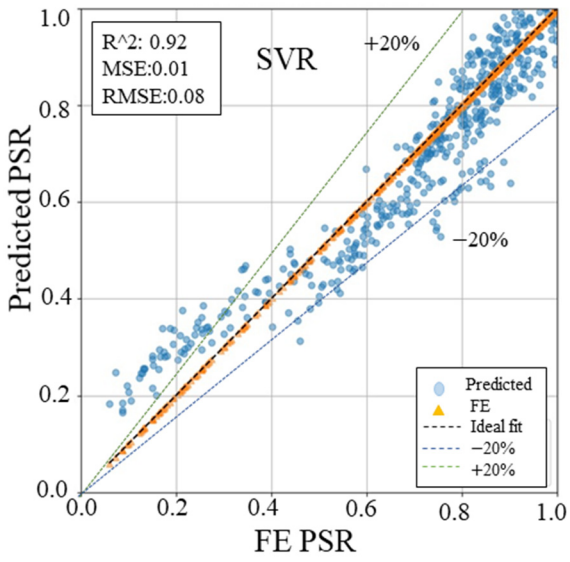

(**d**)

Figure 14. Prediction results of ML methods: (**a**) XGBoost; (**b**) CART; (**c**) ANN; (**d**) SVR.

The comparison of 10 randomly selected plane–strain ratio (PSR) datapoints, shown in Table 9, with extreme gradient boosting (XGBoost), classifical and regression tree (CART), artificial neural networks (ANNs), and support vector regression (SVR) prediction models is shown in Figure 15. It can be seen that the XGBoost and CART prediction models were more consistent with the finite element (FE) and PSR data compared with the other 2 methods (ANN and SVR).

Table 9. Parametric data examples.

Features	A	B	C	D	E	F	G	H	I	J
Slope angle	0	0	0	10	34	0	0	10	10	20
Nailed wall angle	0	0	10	10	5	10	5	0	5	0
Excavation depth	16	28	25	28	13	19	16	22	28	13
Nail length	1.00	1.25	0.75	0.75	1.25	0.50	0.75	1.25	1.25	1.25
Distance from the corner	0.5	2.0	0.5	0.5	1.5	0.0	1.0	0.0	1.0	2.5

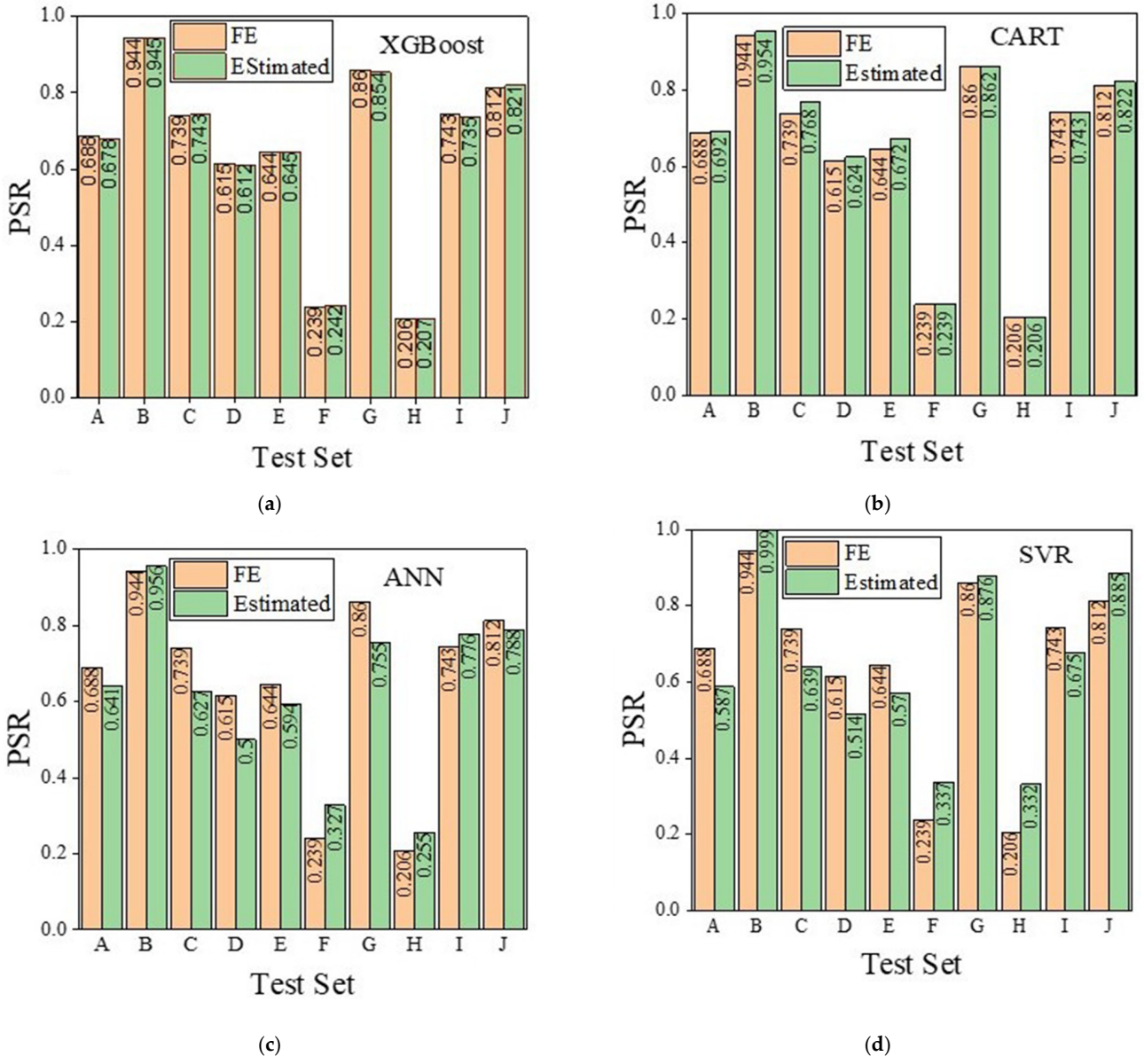

(**a**) (**b**)

(**c**) (**d**)

Figure 15. Comparison between ML prediction and FE for PSR of parametric data samples: (**a**) XGBoost; (**b**) CART; (**c**) ANN; (**d**) SVR.

Permutation importance analysis was performed on extreme gradient boosting (XGBoost) and classifical and regression tree (CART), where the highest performance was achieved. For plane–strain ratio (PSR) estimation, the relative percentage importance of the input parameters distance from the corner (xH), nail length (L/H), excavation depth (H), wall angle (α), and slope angle (β) were listed as 88, 12, 5, 9, and 9, respectively, according to CART. According to the XGBoost prediction model, the importance percentages were 86%, 1%, 1%, 1%, and 10%, respectively. xH was significantly reflected in both models for PSR prediction, as shown in Figure 16. For the XGBoost model prediction, the β factor was the second-most-important parameter after xH. For the CART model prediction, after xH, the L/H, β, and α factors are of relative importance. These results are consistent with the correlation analysis results.

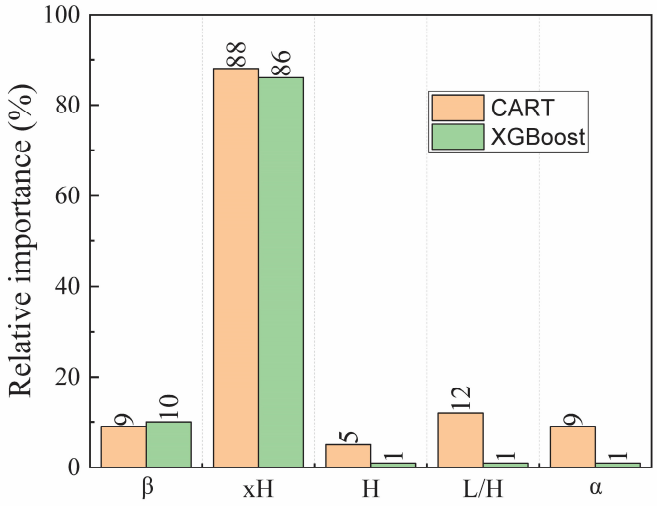

Figure 16. Relative importance of PSR prediction parameters with machine learning methods.

To summarize, in the plane–strain ratio (PSR) estimation phase of this study, the related effects of distance from the corner (xH), nail length (L/H), slope angle (β), wall angle (α), and excavation depth (H) on the PSR value of soil nailed walls were explained. A prediction model combining these five features for PSR prediction of soil nailed walls has not been developed before. The developed models effectively captured the contribution of these features to the PSR value.

6. Conclusions

This study investigates the corner effect, defined as the plane–strain ratio (PSR), on soil nailed walls using Plaxis v.23 software. In the initial stage, displacement analyses were conducted using 25 three-dimensional (3D) models and 25 plane–strain slice models. This stage aimed to determine the impact of excavation pit dimensions on the corner effect. In the second stage, displacement analyzes were performed on 336 3D models and 336 plane–strain slice models depending on four variable factors, and 1610 data points were obtained from the analysis results. The analysis results were evaluated to determine how and in which direction the parameters affected the PSR value. Then, a PSR estimation study was carried out using machine learning methods. The results obtained from the studies are as follows:

- It was observed that the secondary wall had no effect on the excavation pit dimensions in the nailed retaining systems (H = 10 m) used in hard clay soils. It was observed that the primary wall exhibited a greater corner effect, especially under conditions of short wall length (20 m). However, if the primary wall length was 40 m or longer, the plane–strain ratio (PSR) increase graphs were equal. The PSR value reached its maximum level at a distance of 3H from the corner;

- The corner effect increased with the increase in slope angle (β) and excavation depth (H), because these factors decreased the stiffness of the nailed wall. Conversely, increasing the nail length (L/H) and wall angle (α) increased the stiffness and decreased the corner effect;
- A very strong relationship was obtained between the plane–strain ratio (PSR) and the distance from the corner (xH) on the nailed wall, with a correlation coefficient of 0.83. This was followed by a negative relationship between PSR and the slope angle (β);
- Plane–strain ratio (PSR) prediction was performed using machine learning models and extreme gradient boosting (XGBoost), and classifical and regression tree (CART) achieved excellent performance results with an R^2 value of 0.99. The predictions were compared with the results of the finite element analysis, and compatible predictions were obtained.

This study conducted a comprehensive parametric analysis of the corner effect on soil-nailed walls and developed machine learning (ML) models for predicting plane–strain ratio (PSR) values. In this way, designs can be realized by taking into account the corner effect under different slope angle (β), wall angle (α), excavation depth (H), and nail length (L/H) conditions on nailed walls in hard clay soils. Consequently, in areas where corner effects may occur during the design phase, the nail length can be reduced or nail spacing can be increased. Modeling and analysis with the finite element method sometimes requires a solution process that takes days. With trained and proven reliable machine learning methods, these times have been reduced to seconds and 99% accuracy has been proven.

Author Contributions: Conceptualization, S.P. and İ.V.; methodology, S.P. and İ.V.; software, S.P.; validation, İ.V.; formal analysis, S.P.; investigation, S.P.; resources, İ.V.; data curation, S.P.; writing—original draft preparation, S.P.; writing—review and editing, İ.V.; visualization, S.P.; supervision, İ.V.; project administration, İ.V.; funding acquisition, İ.V. All authors have read and agreed to the published version of the manuscript.

Funding: This work was supported by Scientific Research Project Coordination Unit of Sakarya University of Applied Sciences. Project Number: 054-2021.

Institutional Review Board Statement: Not applicable.

Informed Consent Statement: Not applicable.

Data Availability Statement: Data are contained within the article. The data presented in this study can be requested from the authors.

Acknowledgments: All the pertinent data for the soil nailed wall case study presented in this paper were provided by Zetas Zemin Teknolojisi A.S.

Conflicts of Interest: The authors declare no conflicts of interest.

References

1. Carder, D.R. *Ground Movements Casued by Different Embedded Retaining Wall. Constructions Techniques*; Transport Research Board, 1995. Available online: http://worldcat.org/issn/09684107 (accessed on 1 June 2024).
2. Clarke, B.G.; Wroth, C.P. Analysis of Dunton Green Retaining Wall Based on Results of Pressuremeter Tests. *Géotechnique* **1984**, *34*, 549–561. [CrossRef]
3. Ou, C.-Y.; Lai, C.-H. Finite-element analysis of deep excavation in layered sandy and clayey soil deposits. *Can. Geotech. J.* **1994**, *31*, 204–214. [CrossRef]
4. Wong, I.H.; Poh, T.Y.; Chuah, H.L. Performance of excavations for depressed expressway in Singapore. *J. Geotech. Geoenviron. Eng.* **1997**, *123*, 617–625. [CrossRef]
5. Byrne, R.J.; Cotton, D.; Porterfield, J.; Wolschlag, C.; Ueblacker, G. *Manual for Design and Construction Monitoring of Soil Nail Wall*; FHWA-SA-96-069R; Federal Highway Administration: Washington, DC, USA, 1998. Available online: https://rosap.ntl.bts.gov/view/dot/54082 (accessed on 2 June 2024).
6. Clouterre. Recommendations Clouterre 1991: Soil Nailing Recommendations for Designing, Calculating, Constructing and Inspecting Earth Support Systems Using Soil Nailing, Federal Highway Administration Washington, 1991. Available online: https://ntrl.ntis.gov/NTRL/dashboard/searchResults/titleDetail/PB94109980.xhtml (accessed on 2 June 2024).

7. Lazarte, C.A.; Elias, V.; Sabatini, P.J.; Espinoza, R.D. Federal Highway Administration. Office of Technology Applications Geotechnical Engineering Circular No. 7—Soil Nail Walls, Transportation Research Board, 2003. Available online: https://rosap.ntl.bts.gov/view/dot/50250 (accessed on 1 June 2024).
8. Lazarte, C.A.; Robinson, H.; Gómez, J.E.; Baxter, A.; Cadden, A.; Berg, R. *Geotechnical Engineering Circular No. 7 Soil Nail Walls Reference Manual*, 7th ed.; Geotechnical Engineering Circular No. 7; Federal Highway Administration and National Highway Institute: Washington, DC, USA, 2015; NHI-14-007. Available online: https://www.fhwa.dot.gov/engineering/geotech/pubs/nhi14007.pdf (accessed on 1 June 2024).
9. Phear, A.; Dew, C.; Ozsoy, B.; Wharmby, N.J.; Judge, J.; Barley, A.D. Soil Nailing—Best Practice Guidance; Critical Issue in Transportation for 2024 and Beyond, Transportation Research Board, 2005. Available online: http://worldcat.org/isbn/0860176371 (accessed on 1 June 2024).
10. Esmaeili, F.; Varshosaz, M.; Saadatseresht, M. Displacement measurement of soil nail walls using close range photogrammetry. *Procedia Eng.* **2013**, *54*, 516–524. [CrossRef]
11. Jalota, S.; Tangri, A. Comparative study of various flexible facing materials for soil nailed slopes. *Mater. Today Proc.* **2021**, *49*, 2342–2347. [CrossRef]
12. Rabie, M. Performance of hybrid MSE/soil nail walls using numerical analysis and limit equilibrium approaches. *HBRC J.* **2016**, *12*, 63–70. [CrossRef]
13. Zhang, M.; Song, E.; Chen, Z. Ground movement analysis of soil nailing construction by three-dimensional (3-D) finite element modeling (FEM). *Comput. Geotech.* **1999**, *25*, 191–204. [CrossRef]
14. Yuan, J.; Lin, P.; Huang, R.; Que, Y. Statistical evaluation and calibration of two methods for predicting nail loads of soil nail walls in China. *Comput. Geotech.* **2019**, *108*, 269–279. [CrossRef]
15. Esmaeili, F.; Varshosaz, M.; Ebadi, H. Displacement measurement of the soil nail walls by using close range photogrammetry and introduction of CPDA method. *Measurement* **2013**, *46*, 3449–3459. [CrossRef]
16. Fan, C.-C.; Luo, J.-H. Numerical study on the optimum layout of soil–nailed slopes. *Comput. Geotech.* **2008**, *35*, 585–599. [CrossRef]
17. Zhou, Y.D.; Cheuk, C.Y.; Tham, L.G. Numerical modelling of soil nails in loose fill slope under surcharge loading. *Comput. Geotech.* **2009**, *36*, 837–850. [CrossRef]
18. Zevgolis, I.E.; Daffas, Z.A. System reliability assessment of soil nail walls. *Comput. Geotech.* **2018**, *98*, 232–242. [CrossRef]
19. Ghareh, S. Parametric assessment of soil-nailing retaining structures in cohesive and cohesionless soils. *Measurement* **2015**, *73*, 341–351. [CrossRef]
20. Oliaei, M.; Norouzi, B.; Binesh, S.M. Evaluation of soil-nail pullout resistance using mesh-free method. *Comput. Geotech.* **2019**, *116*, 103179. [CrossRef]
21. Rawat, S.; Gupta, A.K.; Kumar, A. Pullout of soil nail with circular discs: A three-dimensional finite element analysis. *J. Rock Mech. Geotech. Eng.* **2017**, *9*, 967–980. [CrossRef]
22. Su, L.-J.; Yin, J.-H.; Zhou, W.-H. Influences of overburden pressure and soil dilation on soil nail pull-out resistance. *Comput. Geotech.* **2010**, *37*, 555–564. [CrossRef]
23. Villalobos, S.A.; Villalobos, F.A. Effect of nail spacing on the global stability of soil nailed walls using limit equilibrium and finite element methods. *Transp. Geotech.* **2021**, *26*, 100454. [CrossRef]
24. Mohamed, M.H.; Ahmed, M.; Mallick, J.; AlQadhi, S. Finite element modeling of the soil-nailing process in nailed-soil slopes. *Appl. Sci.* **2023**, *13*, 2139. [CrossRef]
25. Ye, X.; Wang, S.; Wang, Q.; Sloan, S.W.; Sheng, D. Numerical and experimental studies of the mechanical behaviour for compaction grouted soil nails in sandy soil. *Comput. Geotech.* **2017**, *90*, 202–214. [CrossRef]
26. Wei, W.B.; Cheng, Y.M. Soil nailed slope by strength reduction and limit equilibrium methods. *Comput. Geotech.* **2010**, *37*, 602–618. [CrossRef]
27. Ou, C.-Y.; Chiou, D.-C.; Wu, T.-S. Three-dimensional finite element analysis of deep excavations. *J. Geotech. Eng.* **1996**, *122*, 337–345. [CrossRef]
28. Hsiung, B.-C.B.; Yang, K.-H.; Aila, W.; Hung, C. Three-dimensional effects of a deep excavation on wall deflections in loose to medium dense sands. *Comput. Geotech.* **2016**, *80*, 138–151. [CrossRef]
29. Zad, A.; Farnegin, M. Three Dimensional Analysis of Corner Effects of Deep Excavations Using Soil Nailing Method. International Society for Soil Mechanics and Geotechnical Engineering, 2017. Available online: https://www.issmge.org/uploads/publications/1/45/06-technical-committee-11-tc205-22.pdf (accessed on 1 June 2024).
30. Liu, L.; Wu, R.; Congress, S.S.C.; Du, Q.; Cai, G.; Li, Z. Design optimization of the soil nail wall-retaining pile-anchor cable supporting system in a large-scale deep foundation pit. *Acta Geotech.* **2021**, *16*, 2251–2274. [CrossRef]
31. Chen, Y.; Xu, Y.; Jamhiri, B.; Wang, L.; Li, T. Predicting uniaxial tensile strength of expansive soil with ensemble learning methods. *Comput. Geotech.* **2022**, *150*, 104904. [CrossRef]
32. Ebid, A.M. 35 years of (AI) in geotechnical engineering: State of the srt. *Geotech. Geol. Eng.* **2021**, *39*, 637–690. [CrossRef]
33. Benayoun, F.; Boumezerane, D.; Bekkouche, S.R. Techniques for optimizing parameters of soil nailed vertical cut. *Sel. Sci. Pap. J. Civ. Eng.* **2021**, *16*, 131–145. [CrossRef]
34. Ghaemi, A.; Karimi Dehnavi, M.; Khoshraftar, Z. Exploring artificial neural network approach and RSM modeling in the prediction of CO_2 capture using carbon molecular sieves. *Case Stud. Chem. Environ. Eng.* **2023**, *7*, 100310. [CrossRef]

35. Hebb, D.O. *The Organization of Behavior: A Neuropsychological Theory*, 1st ed.; Psychology Press: New York, NY, USA, 1949; ISBN 978-1-4106-1240-3. Available online: https://www.academia.edu/2279394/The_organization_of_behavior_a_neuropsychological_theory (accessed on 1 June 2024).
36. Hopfield, J.J. Neural networks and physical systems with emergent collective computational abilities. *Proc. Natl. Acad. Sci. USA* **1982**, *79*, 2554–2558. [CrossRef]
37. Widrow, B.; Winter, R.; Baxter, R.A. Learning Phenomena in Layered Neural Networks. In Proceedings of the IEEE First Annual International Conference on Neural Networks, San Diego, CA, USA, 21–24 June 1987.
38. Ombres, L.; Aiello, M.A.; Cascardi, A.; Verre, S. Modeling of steel-reinforced grout composite system-to-concrete bond capacity using artificial neural networks. *J. Compos. Constr.* **2024**, *28*, 04024034. [CrossRef]
39. Dietterich, T.G. Ensemble Methods in Machine Learning. In Proceedings of the Multiple Classifier Systems, Cagliari, Italy, 21–23 June 2000; Springer: Berlin/Heidelberg, Germany, 2000; pp. 1–15. Available online: https://dl.acm.org/doi/10.5555/648054.743935 (accessed on 1 June 2024).
40. Isleem, H.F.; Zewudie, B.B.; Bahrami, A.; Kumar, R.; Xingchong, W.; Samui, P. Parametric investigation of rectangular CFRP-confined concrete columns reinforced by inner elliptical steel tubes using finite element and machine learning models. *Heliyon* **2024**, *10*, e23666. [CrossRef]
41. Zhang, J.; Ma, G.; Huang, Y.; Sun, J.; Aslani, F.; Nener, B. Modelling uniaxial compressive strength of lightweight self-compacting concrete using random forest regression. *Constr. Build. Mater.* **2019**, *210*, 713–719. [CrossRef]
42. Chen, T.; Guestrin, C. XGBoost: A Scalable Tree Boosting System. In Proceedings of the 22nd ACM SIGKDD International Conference on Knowledge Discovery and Data Mining, San Francisco, CA, USA, 13–17 August 2016; Association for Computing Machinery: New York, NY, USA, 2016. [CrossRef]
43. El Ouadrhiri, F.; Adachi, A.; Mehdaoui, I.; Moussaoui, F.; Fouad, K.; Lhassani, A.; Chaouch, M.; Lahkimi, A. Optimization of hydrochar production from almond shells using response surface methodology, artificial neural network, support vector machine and XGBoost. *Desalination Water Treat.* **2024**, *317*, 100154. [CrossRef]
44. Ing, E.; Su, W.; Schonlau, M.; Torun, N. Support vector machines and logistic regression to predict temporal artery biopsy outcomes. *Can. J. Ophthalmol.* **2019**, *54*, 116–118. [CrossRef] [PubMed]
45. Kiangala, S.K.; Wang, Z. An Effective adaptive customization framework for small manufacturing plants using extreme gradient boosting-XGBoost and random forest ensemble learning algorithms in an industry 4.0 environment. *Mach. Learn. Appl.* **2021**, *4*, 100024. [CrossRef]
46. Kumar, R.; Rai, B.; Samui, P. A comparative study of prediction of compressive strength of ultra-high performance concrete using soft computing technique. *Struct. Concr.* **2023**, *24*, 5538–5555. [CrossRef]
47. Byvatov, E.; Schneider, G. Support vector machine applications in bioinformatics. *Appl. Bioinform.* **2003**, *2*, 67–77. Available online: https://pubmed.ncbi.nlm.nih.gov/15130823/ (accessed on 1 June 2024). [PubMed]
48. Vapnik, V.N. *The Nature of Statistical Learning Theory*; Springer: New York, NY, USA, 1995; p. 314. Available online: https://link.springer.com/book/10.1007/978-1-4757-3264-1 (accessed on 1 June 2024).
49. El Bouchefry, K.; de Souza, R.S. Chapter 12—Learning in big data: Introduction to machine learning. In *Knowledge Discovery in Big Data from Astronomy and Earth Observation*; Skoda, P., Adam, F., Eds.; Elsevier: Amsterdam, The Netherlands, 2020; pp. 225–249. [CrossRef]
50. Durgunoglu, H.T. Performance Evaluations of Soil Nailed Walls in Istanbul Graywatch-Case Anaysis. In Proceedings of the 6th International Conference on Case Histories in Geotechnical Engineering, Arlington, VA, USA, 11–16 August 2008. Available online: https://assets-global.website-files.com/63d0fcf37700711149421763/64a28870474cf5f87002311f_paperno59.pdf (accessed on 1 June 2024).
51. *Plaxis 2D Plaxis 2D Manual (Version 2023)*; Bentley Systems International Limited: Dublin, Ireland, 2023.
52. *Plaxis 3D Plaxis 3D Manual (Version 2023)*; Bentley Systems International Limited: Dublin, Ireland, 2023.
53. Ou, C.-Y.; Shiau, B.-Y. Analysis of the corner effect on excavation behaviors. *Can. Geotech. J.* **1998**, *35*, 532–540. [CrossRef]
54. Wu, C.-H.; Ou, C.-Y.; Tung, N. Corner effects in deep excavations-establishment of a forecast model for Taipei Basin T2 zone. *J. Mar. Sci. Technol.* **2010**, *18*, 1–11. [CrossRef]
55. Whittle, A.J.; Hashash, Y.M.A.; Whitman, R.V. Analysis of deep excavation in Boston. *J. Geotech. Eng.* **1993**, *119*, 69–90. [CrossRef]
56. Giger, M.W.; Krizek, R.J. Stability analysis of vertical cut with variable corner angle. *Soils Found.* **1975**, *15*, 63–71. [CrossRef]
57. Tabur, S. A Study of Convex Corner Effects on Digging Pits. Master's Thesis, Institute of Science, Istanbul Technical University, Istanbul, Turkey, 2014. Available online: http://hdl.handle.net/11527/13940 (accessed on 1 June 2024).
58. Mohamed, A. Design Charts for Soil Nailing. Master's Thesis, Faculty of Engineering-Shobra Benha University, New Benha, Egypt, 2010. Available online: https://www.researchgate.net/publication/294428581_Design_Charts_for_soil_Nailing/citations (accessed on 1 June 2024).
59. Shekar, B.H.; Dagnew, G. Grid Search-Based Hyperparameter Tuning and Classification of Microarray Cancer Data. In Proceedings of the 2019 Second International Conference on Advanced Computational and Communication Paradigms (ICACCP), Gangtok, India, 25–28 February 2019. [CrossRef]
60. Lorenzo, P.R.; Nalepa, J.; Kawulok, M.; Sanchez, L.; Ranilla, J. Particle Swarm Optimization for Hyper-Parameter Selection in Deep Neural Networks. In Proceedings of the GECCO'17: Proceedings of the Genetic and Evolutionary Computation Conference, New York, NY, USA, 1 July 2017; pp. 481–488. [CrossRef]

61. Joseph, V.R. Optimal ratio for data splitting. *Stat. Anal. Data Min. ASA Data Sci. J.* **2022**, *15*, 531–538. [CrossRef]
62. Amor, N.; Noman, M.T.; Petru, M. Prediction of functional properties of nano TiO_2 coated cotton composites by artificial Neural network. *Sci. Rep.* **2021**, *11*, 12235. [CrossRef]